Scripta Materialia 224 (2023) 115117

Contents lists available at ScienceDirect

Scripta Materialia

journal homepage: www.journals.elsevier.com/scripta-materialia

‘Anti-sluggish’ Ti diffusion in HCP high-entropy alloys: Chemical complexity vs. lattice distortions

Sandipan Sen [a,*], Xi Zhang [b], Lukasz Rogal [c], Gerhard Wilde [a], Blazej Grabowski [b], Sergiy V. Divinski [a,**]

[a] Institute of Materials Physics, University of Münster, Wilhelm-Klemm-Str. 10, Münster 48149, Germany
[b] Institute for Materials Science, University of Stuttgart, Pfaffenwaldring 55, Stuttgart 70569, Germany
[c] Institute of Metallurgy and Materials Science, Polish Academy of Sciences, Krakow, Poland

ARTICLE INFO

Keywords:
Diffusion
High-entropy alloy
AlScHfTiZr
HCP crystalline lattice
Sluggish diffusion

ABSTRACT

Self-diffusion of Ti in HCP HfTiZr and AlScHfTiZr multi-principal element alloys is measured using the radiotracer technique and applying the ^{44}Ti isotope. In the temperature interval from 973 K to 1373 K, no systematic deviations from linear Arrhenius temperature dependencies are observed. Alloying equiatomic HfTiZr with Al and Sc enhances Ti diffusion rates and the effect becomes more pronounced with increasing Al content. The Ti diffusivities in the present multi-principal element alloys are found to exceed the values predicted by a simple geometric mean of the Ti diffusion coefficients in the pure metals by orders of magnitude, a phenomenon which we refer to as ‘anti-sluggish’ diffusion. Lattice distortions are speculated to dominate the relative enhancement of Ti diffusion in these HCP high-entropy alloys, inducing the ‘anti-sluggish’ behavior. The experimental findings are supported by ab initio-derived mean squared atomic displacements and potential energy fluctuations in these alloys.

Out of the core effects that have been proposed as salient properties of high entropy alloys (HEAs), the concept of ‘sluggish diffusion’ is the one that is least understood. It was first reported [1] and has been studied most intensively [2–6] in face centred cubic (FCC) CoCrFeMnNi and associated systems. A controversial behavior has been established for the FCC HEAs, with a systematic retardation of the diffusion rates of some elements (e.g., slow diffusing Ni) with an increasing chemical complexity of the alloys and prominent deviations for other elements (e.g., fast diffusing Mn) [3]. Very recently, a non-sluggish behavior was reported for Zr diffusion in body centred cubic (BCC) HfTiZrNbTa and HfTiZrNbV alloys [7]. It is thus safe to say that the enigma of sluggish diffusion is far from being understood completely and that it needs further analytical treatment across other alloys and crystal structures [8].

Rogal et al. [9] have developed a hexagonal close packed (HCP) HEA with the composition of $Al_{15}Hf_{25}Sc_{10}Ti_{25}Zr_{25}$ using ab initio-informed thermodynamic calculations. A very recent ab initio prediction of vacancy energetics in the Al–Hf–Sc–Ti–Zr HCP HEA system and its subsystems [10] revealed higher vacancy concentrations in the HEAs as compared to, e.g., the ternary alloy, indicating that the ’sluggish’ diffusion concept may not be applicable in HCP HEAs.

The present paper represents a further step towards understanding tracer diffusion in multi-principal element alloys. Ti self-diffusion is systematically studied in two quinary HEAs, namely in $Al_{15}Hf_{25}Sc_{10}Ti_{25}Zr_{25}$ (15Al) and $Al_5Hf_{25}Sc_{20}Ti_{25}Zr_{25}$ (5Al), and in an equiatomic ternary, i.e., HfTiZr (3C). For the sake of a complete analysis, diffusion of Ti in α-Hf–1.1 wt.%Zr is measured at two representative temperatures, too. In combination with the literature data on Ti diffusion in unary α-Ti [11] and α-Zr [12], a full data set on the impact of chemical complexity on tracer diffusion in HCP materials is reported for the first time. The experimental data are analysed using ab initio-informed calculations.

The choice of the alloys, especially with respect to the equiatomic ratio of Hf, Ti and Zr, is dictated by a previous thermodynamic analysis [9], such as to be able to investigate alloy compositions with the highest tendency for the formation of simple HCP random solid solutions in the temperature intervals suitable for tracer diffusion studies. The sample preparation and homogenization procedure is described in our previous paper [13] on Co solute diffusion in the HCP HEAs, as well as the results

* Corresponding author.
** Co-corresponding author.
E-mail addresses: ssen@uni-muenster.de (S. Sen), divin@wwu.de (S.V. Divinski).

https://doi.org/10.1016/j.scriptamat.2022.115117
Received 6 June 2022; Received in revised form 7 September 2022; Accepted 13 October 2022
Available online 9 November 2022

of chemical and phase analysis of the disordered HCP phase.

The ^{44}Ti radioisotope (half-life of 60 years) was produced by subjecting tiny rectangular Sc foils to proton irradiation. The foils were dissolved in a dilute HCl solution. The ^{44}Ti isotope and residual Sc were chemically separated using an anion exchange absorption in concentrated HCl and neutralized to form a pH-neutral solution. Few microliters of the water solution were deposited on the samples' surfaces before the diffusion annealing treatments.

In view of the absence of literature data on Ti diffusion in α-Hf, we have measured it at two selected temperatures of 1023 K and 1373 K. Since Hf and Zr have comparable atomic radii and similar electron configurations, Hf is very difficult to purify from Zr. The α-Hf material available for the present study contained about 1.1 wt.% of Zr.

The samples with deposited ^{44}Ti isotope were diffusion-annealed (temperatures and times of the annealing treatments are listed in Table S1 in Supplementary Materials) in silica tubes under purified Ar atmosphere. The penetration profiles were subsequently measured using mechanical sectioning via high-precision parallel grinding. The intensities of the γ-decays (at energies of 68 keV and 78 keV) were determined by a solid NaI detector equipped with a 16 K multi-channel energy discriminator.

Examples of the penetration profiles measured at $T = 1373$ K in all four materials are shown in Fig. 1. All other penetration profiles are of a comparably high quality.

The Gaussian (instantaneous source) solution,

$$C(x,t) = \frac{M}{\sqrt{\pi D t}} \exp\left(-\frac{x^2}{4Dt}\right), \tag{1}$$

was found to be typically applicable to describe the measured concentration profiles, especially in the multi-component alloys. In Eq. (1), $C(x,t)$ is the concentration of the ^{44}Ti tracer at a depth x away from the surface built up during the time t, D is the volume diffusion coefficient, and M is the initial tracer amount. In the case of α-Hf, Fig. 1(b), the penetration profile reveals a second contribution which can be attributed to grain boundary diffusion. In particular, the latter can be accounted for using the Le Claire [14] analysis of the exact Suzuoka solution [15] of the grain boundary diffusion problem, $C(x,t) \propto \exp(-qx^{6/5})$. The parameter q is related to the rate of grain boundary diffusion [16]. In the present study, we are focused on volume diffusion and the grain boundary diffusion parameters are therefore not reported.

The measured volume diffusion coefficients are listed in Table S1 of the Supplementary Materials and plotted against the inverse absolute temperature, $1/T$, and against the inverse homologous temperature, T_m/T, in Fig. 2(a) and (b), respectively. The two measured points of Ti diffusion in α-Hf are also shown for comparison.

For each multi-component system, 3C, 5Al and 15Al, the temperature dependencies of the measured diffusivities follow linear Arrhenius-type functions. The determined pre-exponential factors, D_0, and the activation enthalpies, Q, are listed in Table 1. The melting points, T_m, of the alloys are given in Table 1, too. The melting temperatures were determined in Ref. [13] by the CALPHAD approach using the Thermocalc software (thermocalc.com) applying the SSOL5 database.

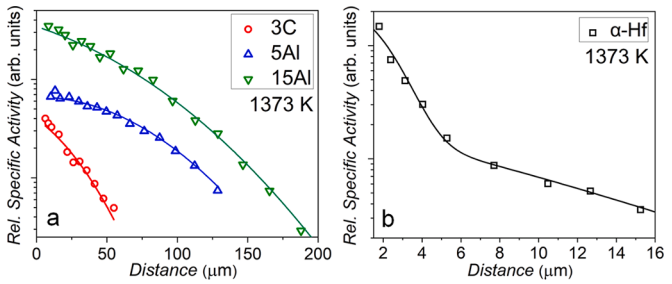

Fig. 1. (a) Penetration profiles for Ti diffusion in 3C (HfTiZr), 5Al ($Al_5Hf_{25}Sc_{20}Ti_{25}Zr_{25}$) and 15Al ($Al_{15}Hf_{25}Sc_{10}Ti_{25}Zr_{25}$). (b) Penetration profile for Ti diffusion in α-Hf. The shown profiles were measured at $T = 1373$ K.

On the absolute temperature scale (Fig. 2(a)), the Ti diffusion rate is highest in the 15Al alloy and it drops with a decreasing Al content in the quinary alloys and becomes even lower in the Al-free equiatomic HfTiZr alloy. On the homologous temperature scale (Fig. 2(b)), an opposite sequence is seen, i.e., Ti diffusion is fastest in the 3C alloy and alloying by Al decelerates Ti diffusion in the quinary alloys, though only slightly.

Furthermore, Fig. 2(a) and (b) substantiate that Ti diffuses faster in the HCP alloys with respect to that in any of the (relevant) unary HCP metals, both on the absolute as well as homologous temperature scales. The Ti diffusivity in the HCP multi-principal element alloys is larger than the hypothetical geometric mean of those in the pure elements (shown in Fig. 2(a) by the dotted line) by orders of magnitude. Since experimentally we do not have any access to the Ti diffusion coefficients in HCP Al or Sc, the estimate of the geometric mean of the unary diffusivities is relevant only for the ternary HfTiZr alloy.

According to the idea of sluggish diffusion, postulated as one of the core effects associated with high entropy alloys [17], the Ti diffusivity should decrease with an increase of the configurational entropy, ΔS_{conf}, described by the ideal mixing entropy as

$$\Delta S_{conf} = -R \sum_{i=1}^{n} X_i \ln(X_i), \tag{2}$$

where X_i is the atomic fraction of the element i in the n-component alloy and R is the universal gas constant.

To corroborate this analysis, the diffusion coefficients of Ti measured at 1373 K (i.e., same absolute temperature) in the HCP systems are plotted as a function of the ideal configurational entropy in Fig. 3 as filled symbols and the Ti diffusivities determined in the HCP systems at $T = 0.75T_m$ (i.e., same homologous temperature) as open symbols.

Fig. 3 demonstrates that the hypothetically anticipated retardation trend, i.e. 'sluggish' diffusion, is not observed in the HCP systems under investigation, neither on the absolute nor on the homologous temperature scale. Most remarkably, the diffusivities of Ti in all three multi-component HCP systems are by orders of magnitude higher than the Ti diffusivities in unary α-Ti (as well as in α-Hf and α-Zr, see Fig. 2(a)). This behavior is anomalous when compared to the observations in FCC [2] and partially in BCC [7] multicomponent systems, where self-diffusivities in multicomponent systems turned out to be lower (FCC [2]) than or similar (BCC [7]) to the diffusivities in the corresponding unaries. This anomalous behavior is termed here as 'anti-sluggish' diffusion.

When analysed at a fixed temperature of 1373 K, even an enhancement of the Ti diffusion rate with an increase of the configurational entropy is seen, Fig. 3(a), confirming the 'anti-sluggish' diffusion behavior of these HCP HEAs. However, such a monotonous dependence would not be seen if the comparison would be done at a lower temperature, below 1000 K, see Fig. 2(a). A further analysis is required.

Using a quasi-chemical model, the fluctuations of the lattice potential energy were proposed [1] to be responsible for the observed 'sluggish' diffusion behavior in FCC multi-component alloys. An increase of the potential energy fluctuations (PEFs) was postulated to lead to the appearance of a larger number of local configurations with enhanced energy barriers for vacancy jumps (traps) which is assumed to impede atomic diffusion [1].

He et al. [18] proposed that the PEFs, x_p, can effectively be decomposed into two contributions, namely chemical, x_{ch}, and elastic, x_e, fluctuations,

$$x_p = x_{ch} + x_e. \tag{3}$$

The chemical contribution is [18]

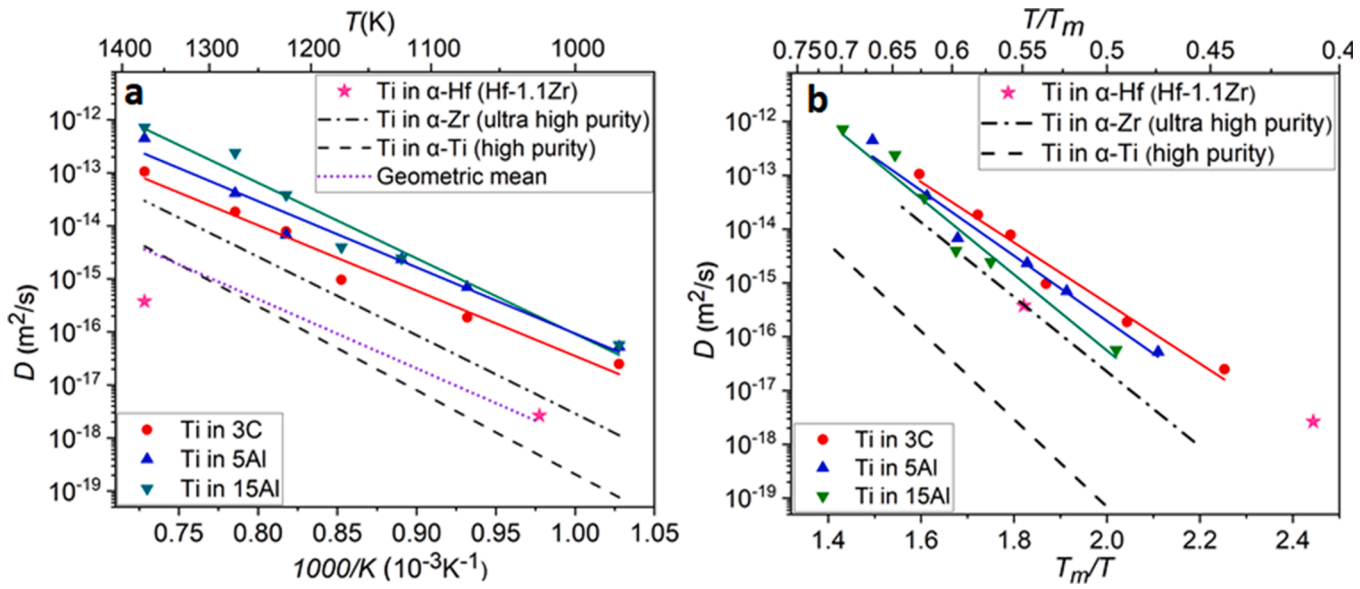

Fig. 2. Arrhenius diagrams for Ti diffusion in the studied HCP systems. Both inverse absolute (a) and homologous (b) temperature scales are used. Ti diffusion in α-Ti (dashed-dotted line [11]), α-Zr (dotted line [12]), α-Hf (violet stars), equiatomic ternary HfTiZr (3C, red circles), and quinary $Al_5Hf_{25}Sc_{20}Ti_{25}Zr_{25}$ (5Al, blue triangles up) and $Al_{15}Hf_{25}Sc_{10}Ti_{25}Zr_{25}$ (15Al, green triangles down) is shown. (For interpretation of the references to color in this figure legend, the reader is referred to the web version of this article).

Table 1
The activation enthalpies, Q, and the pre-exponential factors, D_0, of Ti diffusion in ternary HfTiZr (3C) and quinary $Al_5Hf_{25}Sc_{20}Ti_{25}Zr_{25}$ (5Al) and $Al_{15}Hf_{25}Sc_{10}Ti_{25}Zr_{25}$ (15Al) HCP HEAs. T_m are the melting points of the alloys.

Alloy	T_m (K)	Q (kJ/mol)	D_0 (10^{-4} m^2/s)
3C	2192	235 ± 19	$0.75^{+4.6}_{-0.64}$
5Al	2053	238 ± 20	$2.8^{+21.2}_{-2.4}$
15Al	1956	265 ± 26	162^{+2235}_{-151}

$$x_{ch} = 2\sqrt{\frac{\sqrt{\sum_i \sum_{j,i\neq j} X_i X_j \left(H_{ij}^{mix} - \bar{H}\right)^2}}{k_B T}}, \quad (4)$$

where H_{ij}^{mix} represents the enthalpy of mixing between the i'th and j'th elements, and $\bar{H}$ is the average of H_{ij}^{mix}.

The elastic contribution arises due to a misfit of the atomic sizes of the constituent elements [18],

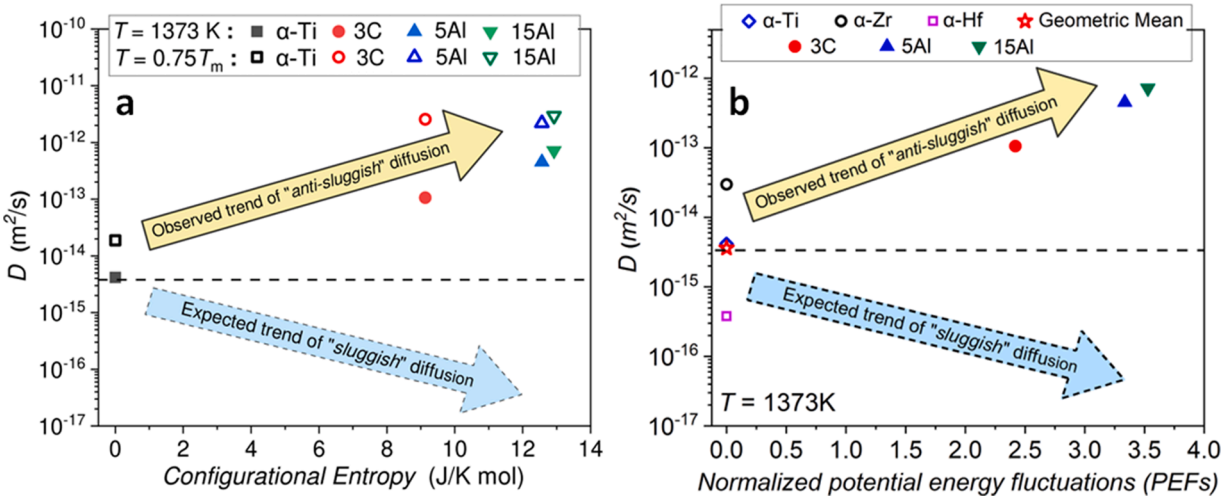

Fig. 3. Diffusion rates of Ti vs. ideal configurational entropy at $T = 1373$ K (closed symbols) and at $T = 0.75T_m$ (open symbols) in the HCP alloys (a) and the Ti diffusion coefficients, D, as function of PEFs at $T = 1373$ K (b).

$$x_e = 3\sqrt{2}\delta \times \sqrt{\frac{\bar{K}\,\bar{V}}{k_B T}}, \tag{5}$$

where δ is an averaged lattice distortion, $\bar{K}$ is the average bulk modulus, and $\bar{V}$ is the average atomic volume. The averaged lattice distortion δ is empirically given by

$$\delta = \sqrt{\sum_{i=1}^{n} X_i \left(1 - \frac{r_i}{\sum_i X_i r_i}\right)^2}, \tag{6}$$

where r_i is the atomic radius of the constituent element i.

The PEFs were estimated for the present HCP multi-component systems according to Eqs. (3)–(6) and by neglecting lattice anisotropy.

Since Al and Sc do not feature HCP phases at ambient conditions, the mixing enthalpies were systematically determined by DFT calculations[1] by employing one special quasirandom structure (SQS) supercell of 96 atoms ($4 \times 4 \times 3$ expansion of the HCP primitive cell) for each sub-binary alloy at the equiatomic composition. For consistency, the total energies of the reference pure elements were calculated using supercells of the same size. The mixing enthalpies per atom were extracted via

$$H_{ij}^{\text{mix}} = H_{ij} - \frac{1}{2}\left(H_i + H_j\right), \tag{7}$$

where H_{ij} refers to the total enthalpy per atom of the sub-binary system $i-j$ (i,j = Al, Hf, Sc, Ti, and Zr) and $H_{i(j)}$ to the total enthalpy per atom of the corresponding pure element.

The atomic radius and bulk modulus for each pure element were extracted from parameterizing the energy-volume curve at 0 K utilizing the Vinet equation of state (EOS) [23]. To obtain the energy-volume curve, for each element, total energies of HCP primitive cells at 11 different volumes were calculated. While the bulk modulus can be directly obtained from fitting the Vinet EOS, the atomic radius R can be estimated utilizing the following relations

$$R = \begin{cases} a/2, & c/a > 1.633, \\ \frac{1}{2}\left(\frac{a^2}{3} + \frac{c^2}{4}\right)^{1/2}, & c/a \le 1.633, \end{cases} \tag{8}$$

where a and c are the HCP lattice constants and $c/a = 1.633$ is the ideal HCP c/a ratio. The such calculated values are listed in Tables 2 and 3.

In Fig. 3(b), the Ti diffusion coefficients in pure α-Ti, α-Zr, α-Hf and in the three multi-component systems are plotted against x_p at $T = 1373$ K. According to the PEF concept [1], there exists an inverse relation between the tracer diffusivity and the PEFs. A comparison of the Ti diffusivities at 1373 K reveals that the diffusion trend is exactly opposite to the one which would be predicted by the PEF theory of 'sluggish' diffusion as indicated by the two arrows in Fig. 3(b) further confirming an anti-sluggish diffusion behavior.

Table 2
Mixing enthalpies for binary pairs in the HCP lattice as determined using the present DFT calculations.

Binary system	H^{mix} (kJ/mol)	Binary system	H^{mix} (kJ/mol)
Al-Sc	−25	Sc-Ti	7
Al-Hf	−21	Sc-Zr	−1
Al-Ti	−26	Hf-Ti	4
Al-Zr	−26	Hf-Zr	0
Sc-Hf	0	Ti-Zr	5

Table 3
Atomic radii and bulk moduli according to the DFT calculations for each unary element in the HCP configuration.

Element	Atomic radius (pm)	Bulk modulus (GPa)
Al	142.9	74.6
Sc	156.7	54.6
Hf	160.8	109
Ti	143.8	113
Zr	159.8	94.3

Table 4
Calculated averaged lattice distortions using Eq. (6).

Alloy	δ (%)
3C	4.50
5Al	4.63
15Al	4.94

Lattice distortions are another inherent property of high-entropy alloys due to the mixing of atoms with different radii on the same lattice [17]. To investigate the impact of lattice distortions, we analyze and compare the averaged lattice distortions δ using Eq. (6), see Table 4. Note that these values enter the expressions for the PEFs via Eq. (5).

One sees immediately that the *element-averaged* lattice distortions follow the order of δ(Ti) < δ(3C) < δ(5Al) < δ(15Al) (obviously, δ(Ti) = 0, and this value is specified for the sake of completeness here). These lattice distortion values however do not depict the distortion of the lattice for particular atomic sites. Since only Ti diffusion is studied in this paper, it is important to compare the distortions of Ti atomic positions and their effect on the observed diffusivity trends.

For this purpose, DFT calculations have been carried out to compute *element-specific* lattice distortions, defined as the mean squared atomic displacements (MSAD) of atomic positions for each element with respect to the undisturbed lattice. DFT ionic relaxations were performed for one 96-atom SQS for each multi-component alloy at zero pressure, i.e., the volume and the cell shape were fully relaxed. The MSAD for each alloying element in each alloy was extracted using

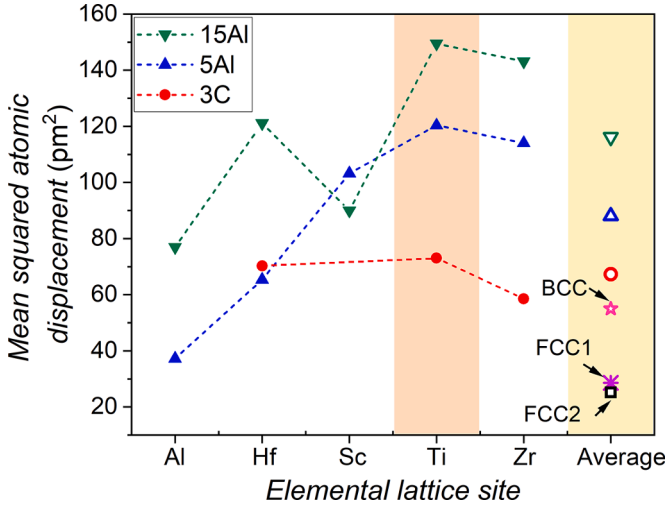

Fig. 4. Lattice distortions defined as mean-squared atomic displacements of the elements with respect to the positions in the undisturbed lattice for the different HCP alloys under investigation as well as for BCC NbMoTaW [24] and FCC CoCrFeMnNi (FCC1 [24] and FCC2 [25]).

[1] All DFT calculations in this work were performed employing the projector augmented wave (PAW) method [19] within the generalized gradient approximation (GGA) in the Perdew–Burke–Ernzerhof (PBE) parametrization [20], as implemented in VASP (version 5.4) [21,22]. The technical details, e.g., the employed PAW potentials, the plane wave cutoff, the number of k-points, and the convergence criterion, are the same as that in Refs. [10,13].

$$\mathrm{MSAD} = \frac{1}{N}\sum_{i} \| \vec{r}_i - \vec{r}_{i,0} \|^2, \quad (9)$$

where $\vec{r}_i$ and $\vec{r}_{i,0}$ represent the relaxed and ideal atomic coordinates of atom i of a given alloying element and N the number of atoms of that element in the alloy. The results of the DFT calculations are shown in Fig. 4.

Whilst the configurational entropy and the PEF analysis performed above failed to provide a conclusive explanation of the experimentally observed diffusion trends, Fig. 4 indicates a substantial clue to explain the diffusion trends.

It can be clearly seen from Fig. 4 that for the Ti atoms the mean-squared atomic displacements are highest for the 15Al alloy followed by the 5Al alloy while the 3C alloy features the lowest values among these three. The enhancement of Ti diffusion in these HCP HEAs with respect to the geometric mean of the values for unary metals is in line with the reasoning of Daw and Chandross [26] who have related the accelerated vacancy diffusion with local distortions in the alloys.

In Fig. 4, the calculated average value of the element-specific MSAD (average over all lattice sites) for each alloy is also plotted along with the reported MSADs for FCC-CoCrFeMnNi [24,25] and BCC-NbMoTaW [24] (yellow shaded area). It is clear that the MSADs for the cubic lattices are much smaller than that of the HCP lattice which is a clear indication that contrary to the cubic systems, lattice distortions play a much more significant role than entropy and potential energy factors.

It can also be speculated that the increased lattice distortions involve an increased contribution of the vibrational entropy to the frequency of atomic jumps during diffusion leading to increasing diffusivity with increasing lattice distortions. A proof of this hypothesis could be a subject of further investigations.

In conclusion, we found that the investigated HCP alloys, i.e., HfTiZr, $Al_5Hf_{25}Sc_{20}Ti_{25}Zr_{25}$ and $Al_{15}Hf_{25}Sc_{10}Ti_{25}Zr_{25}$, feature significantly higher Ti diffusivities with respect to the relevant unary HCP metals as well as their geometric mean, revealing an 'anti-sluggish' diffusion behavior, which is completely opposite to the 'sluggish' diffusion claimed to be a core effect of high-entropy alloys. Both *element-averaged* lattice distortions δ and *element-specific* lattice distortions (MSAD) play a significant role in explaining the anti-sluggish behavior of Ti in the HCP HEAs.

Declaration of Competing Interest

The authors declare that they have no known competing financial interests or personal relationships that could have appeared to influence the work reported in this paper.

Acknowledgments

Financial support from the Deutsche Forschungsgemeinschaft (DFG) via the research projects DI 1419/17-1 and GR 3716/5-1 is gratefully acknowledged. X.Z. and B.G. acknowledge support by the state of Baden-Württemberg through bwHPC and the German Research Foundation (DFG) through grant no. INST 40/467-1 FUGG (JUSTUS cluster) and by the Stuttgart Center for Simulation Science (SimTech).

Supplementary material

Supplementary material associated with this article can be found, in the online version, at doi:10.1016/j.scriptamat.2022.115117

References

[1] K. Tsai, M. Tsai, J. Yeh, Acta Mater. 61 (2013) 4887–4897.
[2] M. Vaidya, K. Pradeep, B. Murty, G. Wilde, S. Divinski, Acta Mater. 146 (2018) 211–224.
[3] J. Kottke, D. Utt, M. Laurent-Brocq, A. Fareed, D. Gaertner, L. Perrière, L. Rogal, A. Stukowski, K. Albe, S.V. Divinski, G. Wilde, Acta Mater. 194 (2020) 236–248.
[4] D. Gaertner, J. Kottke, Y. Chumlyakov, F. Hergemöller, G. Wilde, S.V. Divinski, Scr. Mater. 187 (2020) 57–62.
[5] Dabrowa J., Danielewski M., Metals 10 (3) (n.d.) 347.
[6] A. Mehta, Y. Sohn, Mater. Res. Lett. 9 (5) (2021) 239–246.
[7] J. Zhang, C. Gadelmeier, S. Sen, R. Wang, X. Zhang, Y. Zhong, U. Glatzel, B. Grabowski, G. Wilde, S.V. Divinski, Acta Mater. 233 (2022) 117970.
[8] A. Dash, A. Paul, S. Sen, S. Divinski, J. Kundin, I. Steinbach, B. Grabowski, X. Zhang, Annu. Rev. Mater. Res. 52 (1) (2022) 383–409.
[9] L. Rogal, P. Bobrowski, F. Körmann, S. Divinski, F. Stein, B. Grabowski, Sci. Rep. 156 (2017) 1–17.
[10] X. Zhang, S.V. Divinski, B. Grabowski, Acta Mater. 227 (2022) 117677.
[11] M. Köppers, D. Derdau, M. Friesel, C. Herzig, Defect Diffus, Forum 143 (1997) 43–48.
[12] G. Hood, H. Zou, R. Schultz, E. Bromley, J. Jackman, J. Nucl. Mater. 217 (3) (1994) 229–232.
[13] M. Vaidya, S. Sen, X. Zhang, L. Frommeyer, L. Rogal, S. Sankaran, B. Grabowski, G. Wilde, S. Divinski, Acta Mater. 196 (2020) 220–230.
[14] A.D. LeClaire, Br. J. Appl. Phys. 14 (6) (1963) 351–356.
[15] T. Suzuoka, J. Phys. Soc. Jpn. 19 (6) (1964) 839–851.
[16] A. Paul, L. Tomi, V. Vesa, S. Divinski, Thermodynamics, Diffusion and the Kirkendall Effect in Solids, Springer, 2014.
[17] J. Yeh, S. Chen, S. Lin, J. Gan, T. Chin, T. Shun, C. Tsau, S. Chang, Adv. Eng. Mater. 6 (5) (2004) 299–303.
[18] Q. He, Y. Ye, Y. Yang, J. Appl. Phys. 120 (15) (2016) 154902.
[19] P.E. Blöchl, Phys. Rev. B 50 (1994) 17953–17979.
[20] J.P. Perdew, K. Burke, M. Ernzerhof, Phys. Rev. Lett. 77 (1996) 3865–3868.
[21] G. Kresse, J. Furthmüller, Phys. Rev. B 54 (1996) 11169–11186.
[22] G. Kresse, J. Furthmüller, Comput. Mater. Sci. 6 (1) (1996) 15–50.
[23] P. Vinet, J. Ferrante, J.H. Rose, J.R. Smith, J. Geophys. Res. Solid Earth 92 (B9) (1987) 9319–9325.
[24] N.L. Okamoto, K. Yuge, K. Tanaka, H. Inui, E. George, AIP Adv. 6 (12) (2016) 125008.
[25] M. Masataka, S. Kazuki, A. Hideki, Comput. Mater. Sci. 170 (2019) 109163.
[26] M. Daw, M. Chandross, Phys. Rev. Mater. 5 (4) (2021) 043603.